2020 IEEE/RSJ International Conference on Intelligent Robots and Systems (IROS)
October 25-29, 2020, Las Vegas, NV, USA (Virtual)

A Novel Endoscope Design Using Spiral Technique for Robotic-Assisted Endoscopy Insertion

Wei Li[1], Ya-Yen Tsai[1], Guang-Zhong Yang[2], *Fellow, IEEE* and Benny Lo[1], *Senior Member, IEEE*

***Abstract*— Gastrointestinal (GI) endoscopy is a conventional and prevalent procedure used to diagnose and treat diseases in the digestive tract. This procedure requires inserting an endoscope equipped with a camera and instruments inside a patient to the target of interest. To manoeuvre the endoscope, an endoscopist would rotate the knob at the handle to change the direction of the distal tip and apply the feeding force to advance the endoscope. However, due to the nature of the design, this often causes a looping problem during insertion making it difficult to be further advanced to the deeper section of the tract such as the transverse and ascending colon. To this end, in this paper, we propose a novel robotic endoscope which is covered by a rotating screw-like sheath and uses a spiral insertion technique to generate 'pull' forces at the distal tip of the endoscope to facilitate insertion. The whole shaft of the endoscope can be actively rotated, providing the crawling ability from the attached spiral sheath. With the redundant control on a spring-like continuum joint, the bending tip is capable of maintaining its orientation to assist endoscope navigation. To test its functions and feasibility to address the looping problem, three experiments were carried out. The first two experiments were to analyse the kinematic of the device and test the ability of the device to hold its distal tip at different orientation angles during spiral insertion. In the third experiment, we inserted the device in the bent colon phantom to evaluate the effectiveness of the proposed design against looping when advancing through a curved section of a colon. Results show the moving ability using spiral technique and verify its potential of clinical application.**

I. INTRODUCTION

Gastrointestinal (GI) endoscopy is a common procedure to diagnose and treat diseases in the digestive tract. During the procedure, a long flexible endoscope is served for the purpose and is inserted through a natural pathway, such as oesophagus or colon to the target of interest. The integrated stereo camera can provide the endoscopic view of the target and the instrument channels can provide access to surgical instruments for diagnosis and treatment procedures.

Conventional flexible endoscopes often have limited forward progression ability and Depth of Maximum Insertion (DMI) because the endoscopes are inserted passively into the GI tract. Looping often occurs when the distal tip of the endoscope cannot pass beyond the colon region where there is a large curvature or folding. When this happens, the endoscopist would apply counter pressure, move the patent's body or even attempt for re-insertion. This may expose the patient to higher levels of anaesthesia due to longer procedure and may cause discomfort, internal bleeding or even perforation to the patient. Recent research has indicated that colorectal cancer is ranked as the fourth of the most common cancers and the fifth in cancer-related deaths [1]. Due to its leading cause of morbidity and mortality, there is an increasing demand in endoscopic diagnosis of colorectal cancer which involves colon biopsies at deep colon locations, such as ascending colon, cecum, etc. As such, in the last decades, these have driven the rapid development of novel endoscopic devices with advanced manoeuvrability. Particularly, there has been a growing interest in developing snake-like or flexible robotic endoscopes whose shape can adapt to anatomical structures to avoid collisions to the inner colon wall and resolve looping problem [2], [3].

Fig. 1. Gastrointestinal endoscopy for disease diagnosis and treatment in digestive systems.

A variety of research and commercial robotic systems have been developed for endoscopic interventions. The insertion mechanisms of those systems can be broadly divided into two main streams. One type of endoscopes is the snake-like robot composed of multiple segment structures and hence possesses multiple degrees of freedom (DOFs). Examples to such design include the i^{2}Snake system [4] which used multiple tendon-driven articulated joints for Ear-Nose-Throat surgery; the 5mm diameter customized resectoscope prototype which has three stacked continuum joints by Sarli et al. [5] for trans-urethral surgery; and the snake-like robot, which is based on variable neutral-line mechanism to continuously adjust the stiffness of the continuum joints by varying tensions, proposed by Kim et al. [6]. On the commercial side, the Flex® Robotic System (Medrobotics, Raynham, MA, USA), translated from the HARP system [7], is featured with

[1]Wei Li, Ya-Yen Tsai and Benny Lo are with the Hamlyn Centre for Robotic Surgery, Imperial College London, SW7 2AZ, London, UK {wei.li16, y.tsai17, benny.lo}@imperial.ac.uk
[2]Guang-Zhong Yang is with the Institute of Medical Robotics, Shanghai Jiao Tong University, Shanghai, P.R. China. gzyang@sjtu.edu.cn

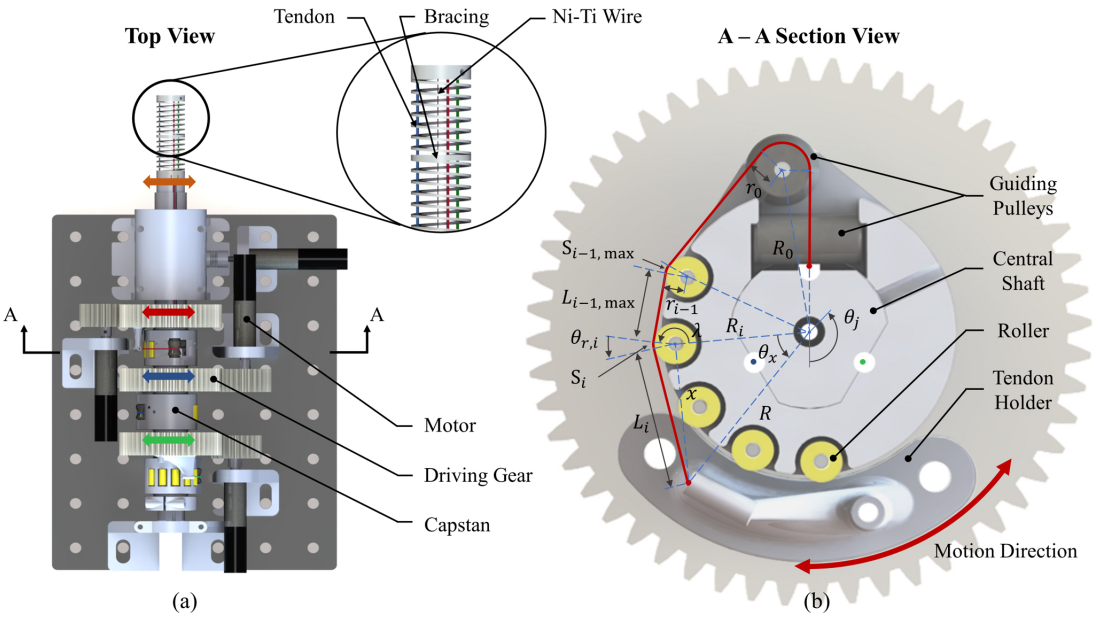

Fig. 2. Conceptual design of the spiral endoscope without flexible body and the main components are labelled. (a) Top CAD view and magnified view of the continuum joint. (b) Section view of a capstan that shows the mechanical play of one tendon. In the sketch, red line represents the tendon and blue dot lines show the geometric relationship.

the design of multi-mechanical and concentric linkages. Relying on the hyper-redundancy mechanisms and follow-the-leader manner, a snake-like endoscope can be manoeuvred and pushed towards the target location while avoiding any injuries due to collisions. The snake-like robots often take the advantages of incorporating multiple joints to increase its flexibility and thus, improves the insertion smoothness and alleviates the potential tearing or scratching of the colon wall. However, many of these designs are based on a rigid passive arm which may limit the DMI for the robots due to early formation of looping and in addition, by including more joints to the device can significantly increase the complexity of the physical design and the control of the system.

Instead of employing the feeding mechanisms from the handle to advance the endoscope, enteroscopes [2] were specifically designed to generate propelling forces at the scope tip to prevent looping formation in small-bowl procedures. A few designs of enteroscopes have been developed including the Single-Balloon Enteroscopy (SBE; Olympus Co., Tokyo, Japan) and Double-Balloon Enteroscopy (DBE; Fujifilm Optical, Saitama, Japan). Both systems have an overtube that can grip and hold to the intestine wall by inflating the enclosed balloons. Spiral Enteroscopy (SE; Spirus Medical, MA, USA), on the other hand, equipped with a spiral-shaped overtube was developed for deep insertion into the small intestine. All these three systems have been evaluated in a number of treatments and results highlighted their diagnostic and therapeutic performance. However, the study has also suggested that the procedures with those enteroscopes are both labour intensive and time consuming during the manual insertion process [8], [9]. To further simplify and expedite the insertion process, a more advanced and reliable system was proposed recently, called PowerSpiral Enteroscopy (PSE; Olympus Co., Tokyo, Japan) [9]. A motorized spiral segment is attached on the shaft to pleat the small bowel onto the enteroscope. Forward or backward rotation of the spiral segment is converted into linear translation for insertion or withdrawal of the endoscope. The smoother and faster rotation movement substantially reduces the procedure time. Nevertheless, the high cost and complication in sterilisation hinders it from wide adoption in clinical use. Apart from these two insertion mechanisms, there is also another very different approach which is the wireless capsule endoscopy known for small-bowel endoscopic evaluation [10]. However, the lack of manoeuvrability to drive towards the desired anatomical sites and functionality to take biopsy specimens are the main drawbacks of this type of system [11].

In this paper, we propose a robotic endoscope design that makes the use of a spiral insertion technique. Compared with the PSE which uses an individual rotate spiral sheath, In our design, the whole shaft of the endoscope can be actively rotated during the insertion, this design provides the crawling ability from the attached spiral sheath, while maintaining the orientation of the distal tip and therefore for easier navigation. Compared with prior works, the proposed scope design has a more compact and simple structure, which is easier for sterilisation and disposable use. The rest of the paper is organized as follows: In Section II, we present the design and the prototype of the proposed device.Section III show the system kinematic, and the control and the manipulation via the tendons. Section IV covers the three experiments and the results followed by the discussion and the conclusion in Section V and VI.

II. Design and Prototyping of an Endoscope using Spiral Technique

A. Concept and methodology

Given the characteristics and limitations of the current enteroscope designs, the spiral design is favoured due to its higher mobility and less structure complexity. Unlike the PSE, which has an independent rotating spiral overtube driven by a torque wire, the proposed robotic endoscope has a fully rotatable body and a novel design of actuation mechanism. It can simultaneously control the bending angle while maintaining the orientation of its tip.

The proposed design concept is inspired by an actuation approach that drives a continuum joint with three tendons to achieve two DoFs bending capability and one DoF rotation around the central axis. To further improve the rotation ability and manoeuvrability of the joint, an alternative solution is to provide one redundant DoF around the central axis, known as in-plane rolling motion. This property is an important feature for robotic instruments, usually achieved by either transmitting the motion to tip [12] or rotating the shaft, such as the da Vinci surgical instruments and μ-IGES [13]. Due to different application requirements, most existing designs only have a maximum of +/-90° in the rolling motion for instrument operation, limited either by the structural design or by the winding pattern of the tendons. Hence, a novel design of actuation mechanism is developed to enhance the shaft rotation capability. The detailed design of the actuation mechanism is presented next in Section II-B, followed by the design and fabrication of the continuum joint in Section II-C.

B. Design of the actuation mechanism

As shown in Fig. 2(a), the actuation mechanism proposed for this endoscope has a rotatable shaft, where the joint is fixed on one side, and the driving gears and capstans are sequentially arranged along the axial direction on the other side. In the circumferential direction, three fixed capstans are equally distributed and the driving gears can revolve freely under the control of the three motors respectively.

The three tendons that control the continuum end-effector are routed through the lumens of the central shaft to the driving unit. Each tendon goes through a pair of pulleys and terminates at the corresponding holder on the driving gears. The tendons are guided with either bowden cables or grooved pulleys with a bending radius larger than 4mm to minimise the occurrence of kicking and permanent deformation. By synchronising the motion between driving gears and central shaft, the rotation differences applied on the tendons can be used to actuate the bending movement of the continuum joint. Detailed control for actuation mechanism is discussed in Section III.

C. Design and fabrication of the continuum joint

The continuum joint design is modified from the work presented in [14], where the design specifications and the strength of the metal printed spring-like joint haven been validated through fatigue experiments and Finite Element Analysis (FEA). To tailor the joint design to achieve multiple DOFs movement, the circular rolling connect is replaced by a central Ni-Ti backbone wire. The selected Ni-Ti wire should be strong enough to resist the compression while flexible enough to closely follow the shape of the central axis during bending. It is also important to avoid the eccentric rotation at bending poses due to the different stiffness between the spring-like structure and the Ni-Ti wire. Hence, a thin layer of bracing is added in the middle of the spring structure. The applied mid-bracing also helps to prevent buckling of the Ni-Ti wire due to its high slenderness ratio.

TABLE I
The specifications of the metal printed continuum joint

Specifications	Values
Number of coil	14
Thickness of coil(mm)	0.6
Maximum Bending angle (°)	180
Diameter (mm)	15
Pitch (mm)	2.8mm

The proposed spring-like continuum joint is 3D printed using selective laser sintering (SLS) technique by the Concept Laser Mlab machine. Stainless steel (CL20ES) was used for prototyping. A summary of the design specifications of the proposed spring-like continuum joint are listed in Table I. The Ni-Ti wire used for the backbone has a diameter of 0.7mm and the tendons used for driving the joint are made of 316 stainless steel, with 0.45mm in diameter and 7x19 strand (ASAHI INTECC CO., Seto, Japan). With the outlined design specifications, the estimated maximum bending angle can reach up to 90°.

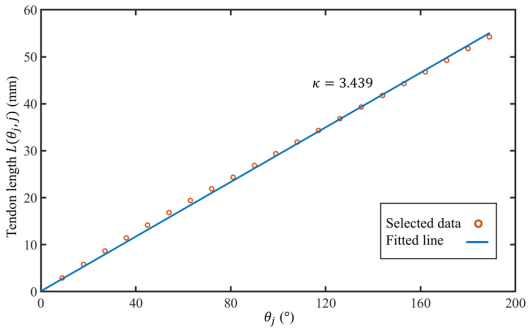

Fig. 3. The estimated linear relationship between the rotating angle θ_j and the total tendon length on the capstan based on the sampled tendon lengths at different rotating angles. Orange circles are the sampling data and the blue line is the fitted linear regression line.

III. Control and Manipulation

A. Mechanical play of the tendons

As mentioned in Section II-B, when the tendon holders have relative motion around the capstans, the lengths of the tendons will change and thus tendons will attach on the

rollers. The correspondence between the rotation angle θ_j and the tendon length $L(\theta_j, j)$ at j^{th} tendon can be calculated based on the CAD model. According to the geometric relationship shown in Fig. 2(b), the length variation of each tendon on the actuation capstans can be described as:

$$L(\theta_j, j) = \begin{cases} \sum_{m=0}^{i-1}(L_{m,\max} + S_{m,\max}) + L_i + S_i, & i = n \\ L_i + S_i, & i = 0 \end{cases}. \quad (1)$$

where n is the index of the last roller in contact with the tendon which can vary from 1 to 5. L_i and S_i represents the euclidean distance and arc length at the i^{th} roller respectively. The values of L_i and S_i can be solved by defining an auxiliary line x,

$$x = \sqrt{R^2 + {R_i}^2 - 2RR_i\cos\theta_x} \quad (2)$$

where θ_x is related to θ_j and substitute x into the following equations,

$$S_i = r_i[2\pi - \lambda - \arccos(\frac{x^2 + {R_i}^2 - R^2}{2xR_i}) + \arctan(\frac{L_i}{r_i})] \quad (3)$$

$$L_i = \sqrt{x^2 - r_i^2},\ i = 0, 1 \cdots n \quad (4)$$

where λ is a fixed value calculated from the geometric relationship of rollers. The next stage $(i+1)$ will begin when the tendon L_i becomes tangential to the $(i+1)^{\text{th}}$ roller, while the tendon length in current stage will become fixed values, written as $L_{i,\max}$ and $S_{i,\max}$. By substituting the values of rotation angles from zero to π, the variation of tendon lengths can be illustrated in Fig. 3. The relationship between θ_j and $L(\theta_j, j)$ can be approximated as linear by fitting a straight line to the sample points. The approximated linear relationship is used to not only simplify the kinematic model, but also to reduce the complexity of joint assembling and initial tendon calibration. The neutral position of tendons is set in a range near the bending angle $\frac{\theta_{j,\max}}{2}$, providing a suitable pre-tension force. As a result, Eq. (1) can be written as

$$L(\theta_j, j) = \kappa\theta_j \quad (5)$$

where κ is the gradient of fitted line labelled in Fig. 3.

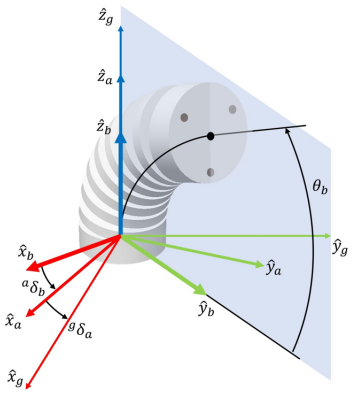

Fig. 4. The kinematic model of a single-segment continuum joint. The origins of three coordinate systems are at the base of the bending section.

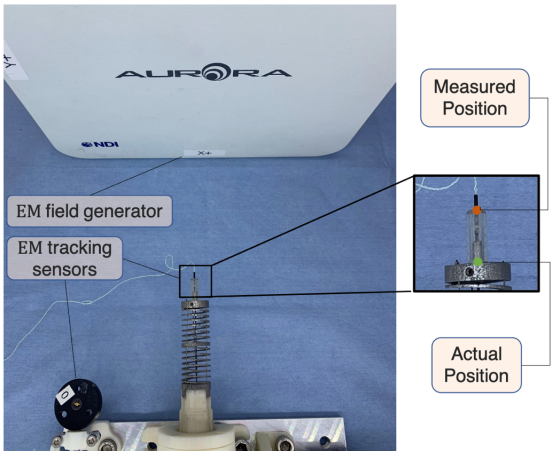

Fig. 5. The experimental setup for the rolling motion validation using a EM tracking system. The disc EM sensor is used as the reference point to keep the sampling data in the same coordinate system. The location measured by the micro EM sensor is marked in red and the actual tip position is marked in green.

B. System kinematics

To derive the pose and orientation of the single joint system, constant curvature based method [15], [16] is implemented as the modelling framework. Fig.4 illustrates the kinematic model in three coordinate systems including global frame $\{g\}$, rotation frame $\{a\}$ and joint frame $\{b\}$. The forward kinematics of the single-joint design can be transformed from the joint frame to the global frame with the position matrix given by

$${}^g\mathbf{R}_b = \frac{L}{\theta_b - \frac{\pi}{2}} \begin{bmatrix} \cos({}^a\delta_b + {}^g\delta_a)(1 - \cos(\theta_b - \frac{\pi}{2})) \\ -\sin({}^a\delta_b + {}^g\delta_a)(1 - \cos(\theta_b - \frac{\pi}{2})) \\ \sin(\theta_b - \frac{\pi}{2}) \end{bmatrix} \quad (6)$$

where L and θ_b define the length and bending angle of the joint respectively. The corresponding orientation transformation can be expressed by

$$\begin{aligned} {}^g\mathbf{R}_b &= {}^g\mathbf{R}_a \cdot {}^a\mathbf{R}_b \cdot {}^b\mathbf{R} \\ &= \mathbf{R}_{\hat{x}o\hat{y}}({}^a\delta_b + {}^g\delta_a) \cdot \mathbf{R}_{\hat{y}o\hat{z}}(\theta_b - \frac{\pi}{2}) \end{aligned} \quad (7)$$

where ${}^g\mathrm{R}_b \in \mathrm{SO}(3)$ is the orientation matrix. As described in Section II-A, to maintain the position and orientation at determined angles corresponding to ω and Θ, when the central shaft is rotating, the redundant solution can be written as

$$\begin{cases} \omega = {}^a\delta_b + {}^g\delta_a \\ \Theta = \theta_b - \frac{\pi}{2} \end{cases} \text{ or } \begin{cases} \omega = {}^a\delta_b + {}^g\delta_a + \pi \\ \Theta = \frac{\pi}{2} - \theta_b \end{cases} \quad (8)$$

where $\omega, \Theta \in (0, 2\pi)$. In order to enforce constraint direction and motion consistency, the second solution is neglected. The configuration vector $\mathbf{\Phi} \in \mathbb{R}^3$ can be given by

$$\mathbf{\Phi} = \begin{bmatrix} \omega & {}^g\delta_a & \Theta \end{bmatrix}^{\mathrm{T}} \quad (9)$$

By using the assumption of constant curvature, the inverse kinematic from an array of configuration variables to tendons

length can be produced as

$$L(\theta_j, j) = r_b \Theta \cos[(\omega - {}^g\delta_a) + (j-1)\gamma], \quad j = 1,2,3 \quad (10)$$

where γ is the angle between equally separated tendons and r_b is the radius from central backbone. Recall Eq. (5), the values of θ_j for actuators can be solved.

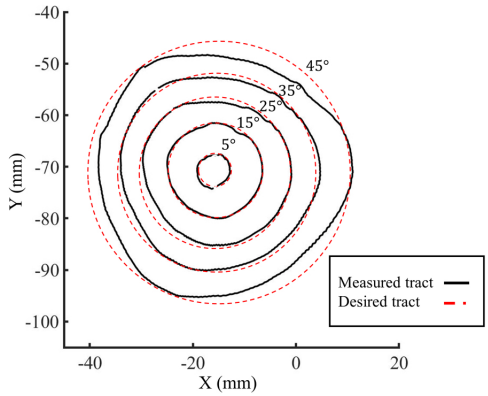

Fig. 6. The comparison between the measured tip trajectories and the desired circular trajectories at several fixed bending angles.

IV. Experiments

To evaluate the functionalities of the endoscope with a rolling tip presented in this paper, three experiments have been conducted. The characteristics of the kinematic motion of the joint were tested in the first two experiments. The performance of an assembled spiral endoscope prototype was validated using an intestine phantom in the last experiment.

A. Position error analysis

To conduct the first and second experiments, a test rig was set up as shown in Fig. 5, which consisted of an Aurora Electromagnetic (EM) Tracking System (Northern Digital Inc, Canada), two EM sensors (one Aurora Micro 6DOF 0.8 mm x 9 mm Sensor and one Aurora 6DOF Reference, 25 mm Disc, Standard sensor). The micro EM sensor was mounted at the tip of the joint to track the position. As illustrated in Fig. 5, there was a small displacement between the sensed location and the actual device tip. The recorded position data was therefore adjusted to reflect such translation.

In the first experiment, the device was set to follow different circular tracks. This was done by bending the device tip at different angles and rotating it about the $\hat{Z}_g$ axis. In this test, the three tendons would have to alternatively change their lengths to maintain the tip at the same position. We have tested a total of 5 different angles at 5°, 15°, 25°, 35° and 45°. With the simple open-loop control, the device was able to follow closely to the desired tracks up to 15°. Then, it started to deviate from the desired tracks as the angles increased. For better visualization, the measured and desired tracks were illustrated in Fig. 6

In the second experiment, the device was validated to see if the proposed design can maintain at a fixed joint tip orientation during spiral insertion. We, again, bent the device at different angles by pulling the three tendons at different lengths. Different from the first experiment, the redundant motion on the shaft will be involved, hence, the joint will keep relatively static about the $\hat{Z}_g$ axis. We have tested different bending angles from the home position, i.e. 0° to 90° with an increment of 10°. We recorded the position error information of the micro EM sensor in relation to the disc EM sensor for a full cycle of axial rotation. Again, with the simple open-loop control, as the bending angles increased, the position error increased. The position error result is shown in Fig. 7. It is worth noting that the position error for each bending angle appears to have 3 clear cycles. This indicates that the tool tip was drawing a small circle at its tip.

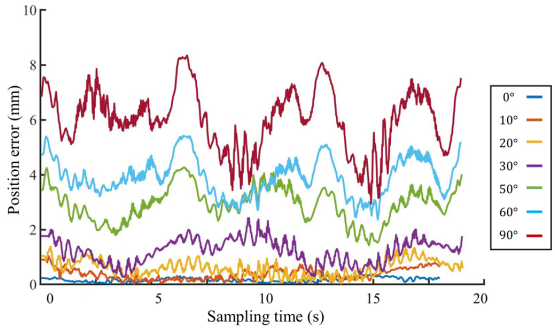

Fig. 7. Position errors at different bending angles when performing the rolling motion at the joint tip for a full circle. The sampling rate is 40Hz.

B. Phantom experiment

The phantom experiment was conducted to test for potential looping problem with the proposed design. In this experiment, we tested our device on a section of intestine phantom which has a diameter of 60*mm* to mimic the curvature and the folding of the real intestine. The actuation unit and continuum joint was connected via a flexible tube. The tube has a length of 600mm and its distal side was covered by a spiral sheath printed using the Elastic 50A resin (Formlabs Inc., USA). The selected material is considered soft enough not to damage the tissue. In addition, an endoscopic camera was attached to the tip of joint to provide visual information.

During the insertion, the endoscope rotated about its axis, while the continuum joint can guide the advance direction and manoeuvre the camera inside the intestine phantom. The advanced motion was done by pleating the phantom wall, where the rotation of spiral sheath are transmitted to linear movement. We tested the insertion and the retrieval by rotating the continuum joint at different directions. From the visual inspection, there was no sign of loop formation during the procedure.

V. Discussion and Future Work

For the first experiment as illustrated in Fig. 6, the deviation increased as the bending angle increased. The same conclusion can also be drawn in the second experiment. Additionally, according to Fig. 7, there were clear periodic

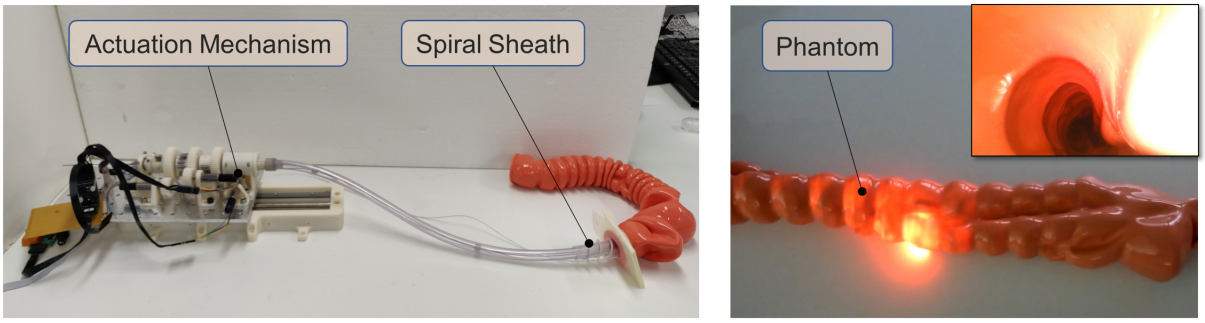

(a) (b)

Fig. 8. (a) The experimental setup for validation on a section of intestine phantom. (b) An enlarged view of the endoscope inside the intestine phantom and the video output.

changes to the position error over the course of full axial rotation. One possible reason could come from the kinematic model that the constant curvature assumption cannot accurately represent the motion of the joint used in this design. It has been investigated that the constant curvature model led to significant errors at large bending angles [17]. Another source of error might be from the overstrained Ni-Ti backbone at a large bending radius, which can be solved by reducing the diameter of backbone. However, in this case, the performance on resisting external axial force would be affected.

In the phantom experiment, the spiral sheath can easily facilitate the advancement of the endoscope during insertion. Although there was no sign of potential looping, the result has shown that the performance was directly affected by the material of the passive tube. Furthermore, due to the weak torsional resistance of passive tube, the torque cannot be fully transmitted from the actuation unit to the joint, resulting in an offset error in the desired orientation and the limited insertion depth.

VI. Conclusion

To conclude, we propose a 4 DOFs (2 DOFs bending, 1 DOF rotation, and 1 DOF axial redundancy) robotic endoscope design by adopting a spiral insertion technique. A novel actuation mechanism is proposed to simultaneously rotate the endoscope shaft and control the bending angle of the joint. The kinematic model is constructed based on constant curvature assumption, however, the position errors show increasing deviation at large bending angles. The proposed design was tested on a section of intestine phantom, and the result showed moving ability using spiral technique, and the potential of the clinical feasibility and usability. In the future works, a better system modelling and control method will be further investigated.

ACKNOWLEDGMENT

The authors would like to thank Shen Treratanakulchai for the help with metal printing.

References

[1] F. Bray *et al.*, "Global cancer statistics 2018: Globocan estimates of incidence and mortality worldwide for 36 cancers in 185 countries," *CA: a cancer journal for clinicians*, vol. 68, no. 6, pp. 394–424, 2018.

[2] H. Yamamoto *et al.*, "Total enteroscopy with a nonsurgical steerable double-balloon method," *Gastrointestinal endoscopy*, vol. 53, no. 2, pp. 216–220, 2001.

[3] J. Burgner-Kahrs, D. C. Rucker, and H. Choset, "Continuum robots for medical applications: A survey," *IEEE Transactions on Robotics*, vol. 31, no. 6, pp. 1261–1280, 2015.

[4] P. Berthet-Rayne *et al.*, "The i 2 snake robotic platform for endoscopic surgery," *Annals of biomedical engineering*, vol. 46, no. 10, pp. 1663–1675, 2018.

[5] N. Sarli *et al.*, "A resectoscope for robot-assisted transurethral surgery," *Journal of Medical Devices*, vol. 10, no. 2, 2016.

[6] Y.-J. Kim *et al.*, "A stiffness-adjustable hyperredundant manipulator using a variable neutral-line mechanism for minimally invasive surgery," *IEEE transactions on robotics*, vol. 30, no. 2, pp. 382–395, 2013.

[7] S. Tully *et al.*, "Shape estimation for image-guided surgery with a highly articulated snake robot," in *IEEE International Conference on Intelligent Robots and Systems*, 2011, pp. 1353–1358.

[8] R. Baniya *et al.*, "Balloon enteroscopy versus spiral enteroscopy for small-bowel disorders: a systematic review and meta-analysis," *Gastrointestinal endoscopy*, vol. 86, no. 6, pp. 997–1005, 2017.

[9] M. Schneider, J. Höllerich, and T. Beyna, "Device-assisted enteroscopy: A review of available techniques and upcoming new technologies," *World journal of gastroenterology*, vol. 25, no. 27, p. 3538, 2019.

[10] G. Iddan *et al.*, "Wireless capsule endoscopy," *Nature*, vol. 405, no. 6785, pp. 417–417, 2000.

[11] A. De Leusse *et al.*, "Video capsule endoscopy for investigation of obscure gastrointestinal bleeding: feasibility, results, and interobserver agreement," *Endoscopy*, vol. 37, no. 07, pp. 617–621, 2005.

[12] A. Schmitz *et al.*, "A rolling-tip flexible instrument for minimally invasive surgery," in *IEEE International Conference on Robotics and Automation*, 2019, pp. 379–385.

[13] J. Shang *et al.*, "A single-port robotic system for transanal microsurgery—design and validation," *IEEE robotics and automation letters*, vol. 2, no. 3, pp. 1510–1517, 2017.

[14] Y. Hu *et al.*, "Design and fabrication of a 3-d printed metallic flexible joint for snake-like surgical robot," *IEEE Robotics and Automation Letters*, vol. 4, no. 2, pp. 1557–1563, 2019.

[15] N. Simaan *et al.*, "Design and integration of a telerobotic system for minimally invasive surgery of the throat," *The International journal of robotics research*, vol. 28, no. 9, pp. 1134–1153, 2009.

[16] B. A. Jones and I. D. Walker, "Practical kinematics for real-time implementation of continuum robots," *IEEE Transactions on Robotics*, vol. 22, no. 6, pp. 1087–1099, 2006.

[17] N. Liu *et al.*, "Design and kinematics characterization of a laser-profiled continuum manipulator for the guidance of bronchoscopic instruments," in *IEEE International Conference on Robotics and Automation*, 2018, pp. 25–31.